IEEE Access
Multidisciplinary ⋮ Rapid Review ⋮ Open Access Journal

Received 23 March 2023, accepted 3 April 2023, date of publication 5 April 2023, date of current version 11 April 2023.

Digital Object Identifier 10.1109/ACCESS.2023.3264906

RESEARCH ARTICLE

Methods for Simplifying Quasi-Deterministic Millimeter-Wave Channel Models

RADWA A. ROSHDY[1], MOSTAFA H. DAHSHAN[2], SALMAN A. ALQAHTANI[3], (Member, IEEE), AHMED EMAM[4], HOSSAM M. KASEM[5], AND MOHAMMED A. SALEM[1], (Member, IEEE)

[1]Department of Electrical Engineering, Higher Technological Institute, 10th of Ramadan City 44629, Egypt
[2]School of Computing, Mathematics and Engineering, Charles Sturt University, Bathurst, NSW 2795, Australia
[3]Department of Computer Engineering, College of Computer and Information Sciences, King Saud University, Riyadh 11543, Saudi Arabia
[4]Faculty of Computer Science and Engineering, King Salman International University (KSIU), El Tor 8701301, Egypt
[5]Department of Electronics and Electrical Communication Engineering, Faculty of Engineering, Tanta University, Tanta 31512, Egypt

Corresponding author: Mohammed A. Salem (mohammed.adel@hti.edu.eg)

This work was supported by King Saud University, Riyadh, Saudi Arabia, under Project RSPD2023R585.

ABSTRACT It is crucial to have a dependable and precise channel model in order to study the properties of millimeter wave (mmWave) propagation. The Quasi-deterministic (QD) channel model is employed in this viewpoint, which describes the propagation of mm-Wave as a group of reflected and scattered rays originating from a complex environmental setup. These rays are assumed to travel in clusters, with each cluster consisting of a deterministic ray followed by postcursor rays and preceded by precursor rays. The summation of these rays is the number of multiple path components (MPCs) of each cluster. However, this comes at the cost of higher computational complexity for the channel model, which can hinder the simulation's scalability. To simplify the QD channel model while maintaining accuracy, one option is to decrease the number of MPCs. In this paper, we present an analysis of path gains (PGs) of specular and diffused rays to reduce the total number of MPCs. Specifically, we propose two different reduction methods namely: i) the reduced post rays (RPR) method ii) the removed surfaces post rays (RSPR) method. The computational performance of the proposed methods is investigated in terms of computational time, and complexity. Additionally, the accuracy validation compared to the original QD model is evaluated in terms of PG cumulative distribution function (CDF), signal-to-noise ratio (SNR), and intra-cluster statistics. The proposed methods' complexity and accuracy were assessed by examining measured data from indoor and outdoor environments at 60 GHz and 28 GHz, respectively. Both first and second-order reflection orders were tested to illustrate the balance between the two variables. The simplified methods suggested can decrease computational time by approximately 16% and 11% for RSPR and RPR schemes, respectively, when compared to the original QD.

INDEX TERMS Diffused rays, millimeter wave propagation, multipath components, path gain, quasi-deterministic channel models, intra-cluster statistics, ray tracer.

I. INTRODUCTION

Millimeter wave (mmWave) participates effectively in the next cellular network generations (e.g., 5G and 6G) deployment. This is because, it can increase communication capacity, improve spectrum efficiency, support massive multiple input multiple output (MIMO) and allow for large Bandwidth (B.W) allocations which are translated directly to higher data rate transfer [1]. Moreover, it can provide a carrier frequency of up to 71 GHz in the future release of the third Generation Partnership Project new radio (3GPP NR) [2]. MmWave technology will play a key role in achieving the desired network performance and communication tasks in both 5G and 6G communication systems [3], [4], [5].

Despite these promising features, mmWave suffers from several challenges including: huge propagation loss, compared to other communication systems that use low carrier frequency, resulting in its sensitivity to atmospheric conditions like rain, humidity, and fog. Consequently, the range of mmWave is limited; it propagates at 200 m [6]. Moreover,

The associate editor coordinating the review of this manuscript and approving it for publication was Adao Silva.

it is sensitive to blockage, and obstacles such as the human body, buildings, and vehicles. For propagation measurements that are conducted in a realistic indoor environment in the presence of human activity, the channel is blocked for about 1% or 2% of the time for 1 to 5 persons [7]. In addition, directional beamforming systems can be achieved. The need for accurate alignment of the transmitter and receiver beams results in a higher controller overhead for managing mobility and estimating channels [8]. As a result, the mmWave channel appears extremely violative to cellular communication systems. However, these challenges are investigated several works. In [9], a novel distributed power was proposed to mitigate the inter-beam interference directors at sub-6 GHz and mm-Wave and achieve high throughput using game theory-based power constraints. A low complexity using quantized hybrid precoding is used in [10] and [11] to improve energy efficiency in MIMO transmission.

A. LITERATURE REVIEW

The literature review discusses three primary models for mmWave channels that vary in their level of complexity, time requirements, and accuracy. The initial analytical channel model is a basic representation of mmWave propagation features, particularly fading, and employs only one random variable described by nakagami-m or Rayleigh distribution [12], [13]. It can be used in combination with sectorized beamforming for line of sight (loS) transmission. Despite its simplicity, this model does not accurately address antenna arrays and beamforming techniques [14]. Analytical methods are used in various literary works to develop mmWave channel models. For instance, a 3D Uplink Channel model for mmWave front haul links was presented in [15] for small cell networks of the future. In [16], a stochastic channel model based on temporal and spatial statistics was introduced to generate the channel impulse response (CIR). Additionally, [17] featured an analytical performance study of two heterogeneous networks that operate simultaneously at the same time, space, and frequency domains.

The second is the stochastic spatial channel model (SCM) in which the channel model is characterized by generating multiple path components (MPCs) from several random distributions. The parameters of these distributions are specified by statistical fits on channel measurements [18]. With the aid of these parameters, the SCM can address large-scale fading and fast-fading phenomena [19]. WINNER, WINNER-II, and NYU models are the most significant examples of SCM and are also available with open-source simulators [20], [21].

The third type of channel model is known as the quasi-deterministic (QD) model. This approach involves using a ray tracer (RT) to generate multipath components (MPCs) based on the propagation environment's geometry [22]. These MPCs provide information about various channel parameters, including delay, path gain, angle of arrival (AoA), and angle of departure (AoD) [23]. Depending on whether the transmission is line-of-sight (LoS) or non-line-of-sight (NLoS), the MPCs may consist of direct ray components or diffused ray components resulting from scattering surfaces in the environment [24].

However, NLoS contributions on single or multiple bounces e.g., on metal objects are not with diffused rays [25]. The diffused rays are generated by using a stochastic model and rely on the surface roughness on which rays reflect and are clustered around the main reflected component [22], [26].

Although the QD channel model provides a reliable and accurate channel model. Additionally, it is more computationally complex, especially if the number of reflecting and scattering surfaces is large for a given scenario [24]. The complexity of the QD channel model is typically linked to the quantity of generated MPCs and the number of antennas at both the transmitter and receiver [27]. Therefore, decreasing either the number of MPCs or antennas can reduce the complexity of the channel model, as long as accuracy is maintained with minimal reduction The QD channel model was simplified in [24] and [28] by focusing only on MPCs that had a received power exceeding a specific threshold, which was determined based on the most powerful MPC. In [27], the SCM channel model was simplified by removing clusters and sub-paths (i.e., spatial components of the channel). The effectiveness of these simplified approaches was assessed using both signal interference to noise ratio (SINR) and computation time.

B. MOTIVATION AND CONTRIBUTIONS

The QD channel model is effective in providing precise channel parameter characterization for mmWave technology. However, its computational complexity limits the scalability of the simulator. To address this issue, a simplified QD mmWave channel model that maintains accuracy is necessary. The proposed solution involves reducing the number of MPCs to simplify the QD channel model while minimizing any impact on its accuracy.

The main contributions of this paper are summarized as follows:

1) We offer an evaluation of the path gains (PG) of specular and diffused rays in both indoor and outdoor settings - specifically, a data center and parking lot - at frequencies of 60 GHz and 28 GHz. This analysis pertains to both first and second reflection orders.
2) This analysis suggests two distinct approaches for reducing MPCs by eliminating those with the lowest path gains. The RPR and RSPR methods are introduced as the first and second options, respectively. Both methods involve removing MPCs with weaker PGs to reduce their overall number.
3) The main focus of this study is removing MPCs that have the weakest path gains, removing surface post rays and removing the MPCs. The aim was to compare the effectiveness of these reduction methods to the QD model in terms of reducing computational time and complexity, as well as improving channel model accuracy in areas such as PG CDF, SNR, K-factor,

power delay decay, delay spread, and angular spread within clusters.

4) We present a comparison with other simplified channel models in literature review. Moreover, present a complexity and model accuracy tradeoff for the two methods to obtain optimal results for decreasing the simulation computational time and complexity with a nominal reduction in QD channel model accuracy compared to the original QD model.
5) The performance evaluation results demonstrate that the QD channel model can be simplified via either RSPR or RPR with a minimal reduction in accuracy.

The rest of the paper is organized as follows. Section II provides an overview of the mm Wave quasi-deterministic channel model. In Section III, we offer an analysis of how to reduce multipath components (MPCs) using path gain values generated by both specular and diffused rays. We propose two MPCs reduction methods for indoor environments, specifically data centers operating at 60 GHz. In Section IV, we evaluate the effectiveness of these methods using various metrics such as path gain CDF, DDIR, SNR, and computing time for the first and second reflection orders. We summarize the performance evaluation results in Section V and present our conclusion in Section VI.

Notation: Through this paper, light symbols and bold symbols denote to scalar and random variables, respectively. For a given random variable $\mathbf{X}$:

1) $\mathcal{N}(\mu, \sigma^2)$ denotes Normal distribution with "μ" mean and variance "σ^2".
2) $\mathcal{R}(s, \sigma)$ denotes Rician distribution where value of s and σ are positive. It is generated as $\mathbf{X} = \sqrt{\mathbf{Y} + \mathbf{Z}}$ where $\mathbf{Y} \backsim \mathcal{N}(\mu, \sigma^2)$ and $\mathbf{Z} \backsim \mathcal{N}(\mu, \sigma^2)$.
3) $\mathcal{L}((\mu, \sigma^2)$ denotes Laplacian distribution with mean and variance equal to μandσ^2, respectively.
4) $\varepsilon(\varepsilon)$ denotes Exponential distribution with mean and variance equal to $\frac{1}{\varepsilon}$ and $\frac{1}{\varepsilon^2}$, respectively.

II. MMWAVEQUASI-DETERMINISTIC (QD) CHANNEL MODEL

The QD model utilizes ray tracing to analyze the mmWave channel, taking into account both direct (D-ray) and reflected rays based on the transmitter and receiver position and environment geometry. However, diffracted rays are disregarded as they have little impact on mmWave transmission [29]. The direct ray is deterministic (LoS) ray is predictable and doesn't produce any scattered elements. The transmitter and receiver positions are used to determine its characteristics, such as delay, angle of arrival (AoA), and angle of departure (AoD) [22]. In terms of path gain ($\mathbf{PG_0}$), it's computed using the Friis transmission equation in the subsequent way:

$$\mathbf{PG_0} = 20log_{10}(\frac{\varepsilon_c}{4\pi\, l_{ray}}) - \mu_{RL} \tag{1}$$

where ε_c is the carrier frequency wavelength, l_{ray} is the D-ray length from the transmitter to the receiver and μ_{RL} is the mean reflection loss of a given surface.

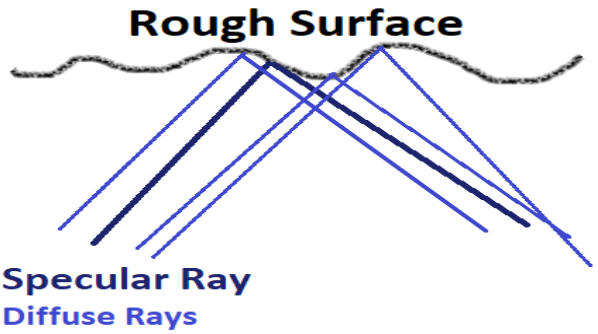

FIGURE 1. Rough surface reflected ray scattering.

In the case of NLoS transmission, the reflected rays are considered. They are also named specular rays and have the strongest path gains, while other rays are produced because of the scattering of specular rays from surfaces that have weaker path gains. These rays are clustered around the specular rays and are named diffuse rays [30]. The path gains of specular rays for n$^{\mathrm{th}}$ reflection order, with (n >1) are given in equation 2.

$$\mathbf{PG_0} = 20log_{10}(\frac{\varepsilon_c}{4\pi\, l_{ray}}) - \sum_{i=1}^{n} \mathbf{RL}_{\mathrm{i,dB}} \tag{2}$$

where $\mathbf{RL}_{\mathrm{i,dB}}$ is the random reflection loss factor given by the reflecting surface's material and is defined by Rician distribution $\mathbf{RL}_{\mathrm{i,dB}} \sim \mathcal{R}(s_{RL,i}, \sigma_{RL,i})$. $(s_{RL,i}, \sigma_{RL,i})$ refers to the statistics related to the material of the i-th reflector of the given ray.

Figure 1 illustrates that multiple diffuse rays accompany each specular ray. Among these diffuse rays, some arrive before the specular ray and are referred to as precursor rays (Npre), while others arrive after it and are called postcursor rays ($\mathrm{N_{post}}$) [31]. The quantity of MPCs within each cluster can be determined by:

$$N_{MPC} = R(N_{pre} + 1 + N_{post}) \tag{3}$$

where R is an integer number denotes the reflection order.

The "1" in (3) means that each cluster has only one specular ray.

The angle of departure (AoD) and angle of arrival (AoA) in azimuth (AZ) and elevation (EL) of MPCs are given by:

$$\mathrm{AoD_{AZ/EL}} = \mathrm{AoD_0} + \alpha_{AoDAZ/EL} \tag{4}$$

where $\mathrm{AoD_0}$ is for the D-ray. $\alpha_{AoDAZ/EL} \backsim \mathcal{L}((0, \boldsymbol{\sigma}^2_{\alpha AoDAZ/EL})$ is the angle spread. The variance $\boldsymbol{\sigma}^2_{\alpha AoDAZ/EL} \backsim \mathcal{R}(s_{\sigma^2_{\alpha AoDAZ/EL}}, \sigma_{\sigma^2_{\alpha AoDAZ/EL}})$ and is obtained independently for each cluster. The angle of arrival (AoA) in azimuth (AZ) and elevation (EL) is obtained by using the same equation in (4).

The intra-cluster parameters are described by a loss factor ($\mathbf{K}$), power delay decay constant (γ), delay spread (ε), power delay constant ($\mathbf{S}$), and angle spread (α).

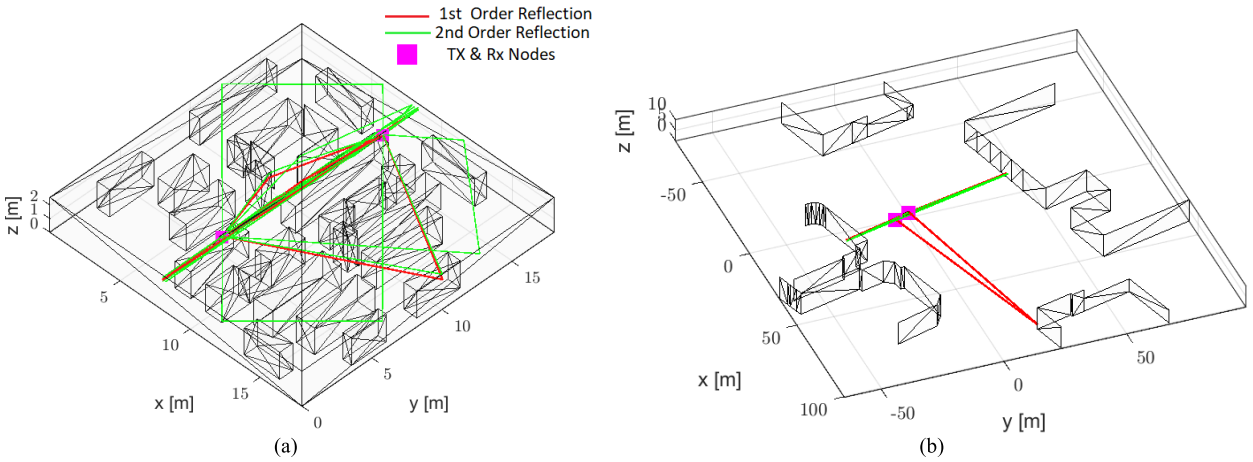

FIGURE 2. Visual representation of used scenarios (a) data center, (b) parking Lot.

The **K**-factor, γ, and ε are randomly generated using the Rician distribution with "s" mean and variance "σ" R(s, σ) [24]. The loss factor **K** is defined as the ratio between the cursor strength and precursor/postcursor diffuse components and is calculated as:

$$K_{pre/post} = \frac{\mathrm{PG_{cursor}}}{\sum_{i=1}^{N} {}_{pre/post}\mathrm{PG_i}} \tag{5}$$

III. THE PROPOSED MPCS REDUCTION ANALYSIS

Once the weakest path gains are known, the next step is to determine which MPCs should be removed. This can be done by calculating the power of the MPCs and then removing the MPCs with the lowest power. The power of the MPCs can be calculated by taking the product of the path gain and the delay spread of the MPCs. The delay spread of the MPCs can be calculated by taking the difference between the maximum and minimum delays of the MPCs. After calculating the power of the MPCs, the weakest MPCs can be identified and removed. In addition to removing the weakest MPCs, another approach to reduce the total number of MPCs is to use a clustering algorithm. Clustering algorithms can be used to group the MPCs into clusters based on their path gains and delay spreads. The clusters can then be merged to reduce the total number of MPCs. This approach can be used to re duce the total number of MPCs while still maintaining the accuracy of the channel model.

The path gains of precursor and postcursor rays are calculated as follows:

$$\mathbf{PG}_{\mathrm{pre,i,dB}} = \mathbf{PG}_{0,\mathrm{dB}} - \boldsymbol{K}_{pre,dB} - \frac{\left|\boldsymbol{\tau}_{i,pre} - \tau_0\right|}{\gamma_{pre}}\left(10log_{10}e\right) + (10log_{10}e)\boldsymbol{S}_{pre} \tag{6}$$

$$\mathbf{PG}_{\mathrm{post,i,dB}} = \mathbf{PG}_{0,\mathrm{dB}} - \boldsymbol{K}_{post,dB} - \frac{\left|\boldsymbol{\tau}_{i,post} - \tau_0\right|}{\gamma_{post}}\left(10log_{10}e\right) + (10log_{10}e)\boldsymbol{S}_{post} \tag{7}$$

where:

- $i = 1, \ldots, \ldots, \ldots, N_{pre/post}$
- $\mathbf{PG}_{0,\mathrm{dB}}$is the path gains of specular rays as mentioned in (2).
- $\mathbf{K}_{\mathrm{pre/post}} \backsim \mathcal{R}(s_{K_{pre/post}}, \sigma_{K_{pre/post}})$.
- $\gamma_{pre/post} \backsim \mathcal{R}(s_{\gamma_{pre/post}}, \sigma_{\gamma_{pre/post}})$.
- $\boldsymbol{S}_{pre/post} \backsim \mathcal{N}(0, \boldsymbol{\sigma}^2_{s,pre/post})$ and $\boldsymbol{\sigma}_{s,pre/post} \backsim \mathcal{R}(s_{\sigma_{s,pre/post}}, \sigma_{\sigma_{s,pre/post}})$.
- τ_0 is the arrival time of the specular ray and is calculated as follows:

$$\tau_0 = \frac{d}{c} \tag{8}$$

  where d is the distance between Tx and Rx and c is the light speed.
- $\boldsymbol{\tau}_{i,pre}$ is the inter arrival time of precursor rays and is given by:

$$\boldsymbol{\tau}_{i,pre} = \tau_o - \sum_{j=1}^{i} \Delta_{j,pre} \tag{9}$$

- $\boldsymbol{\tau}_{i,post}$ is the inter arrival time of postcursor rays and is given by:

$$\boldsymbol{\tau}_{i,post} = \tau_o + \sum_{j=1}^{i} \Delta_{j,post} \tag{10}$$

  where Δ is the arrival rate and is generated randomly using exponential distribution $\varepsilon(\boldsymbol{\varepsilon}_{pre})$ and $\boldsymbol{\varepsilon}_{\mathrm{pre}}$is defined by Rician distribution $\mathcal{R}(s_{\boldsymbol{\varepsilon}_{pre}}, \sigma_{\boldsymbol{\varepsilon}_{pre}})$. The arrival time of postcursor rays is calculated the same as that of precursor rays except that τ_o is added to the sum of the arrival rate.

We perform our analysis on a QD channel realization ray tracer (RT) developed by the national institute of standards and technology (NIST). It is a three-dimensional (3D) RT based on a real measurement campaign which grants a realistic, scalable and flexible channel model [23].

TABLE 1. Data center NIST material library.

		Ceiling	Rack-top	Curtain	Wall and Columns	Rack-sides	Floor
$K_{dB} \sim \mathcal{R}(s,\sigma)$	$(s_{K_{pre}}, \sigma_{Kpre})$	(0,0)	(0,0)	(0,0)	(8.32,5.62)	(6.91,2,62)	(0,0)
	$(s_{K_{post}}, \sigma_{K_{post}})$	(6.12,8.05)	(0,0)	(0.53,6.43)	(6.91,3.64)	(0.2,4)	(6.12,8.05)
$\gamma \sim \mathcal{R}(s,\sigma)$	$(s_{\gamma_{pre}}, \sigma_{\gamma_{pre}})$	(0,0)	(0,0)	(0,0)	(0.12,1.23)	(0.21,2.84)	(0,0)
	$(s_{\gamma_{post}}, \sigma_{\gamma_{post}})$	(0.65,0.34)	(0,0)	(0.69,0.39)	(0.07,2.44)	(0.4,8.34)	(0.65,0.34)
$\sigma_s \sim \mathcal{R}(s,\sigma)$	$(s_{\sigma_{spre}}, \sigma_{\sigma_{spre}})$	(0,0)	(0,0)	(0.23,0.01)	(0.01,0.4)	(0.23,0.25)	(0,0)
	$(s_{\sigma_{spost}}, \sigma_{\sigma_{spost}})$	(0.05,0.39)	(0,0)	(0.86,0.4)	(0.01,0.47)	(0.02,0.54)	(0.05,0.39)
$\lambda \sim \mathcal{R}(s,\sigma)$	$(s_{\lambda_{pre}}, \sigma_{\lambda_{pre}})$	(0,0)	(0,0)	(0,0)	(0.11,2.96)	(0.05,1.15)	(0,0)
	$(s_{\lambda_{post}}, \sigma_{\lambda_{post}})$	(0.63,0.59)	(0,0)	(0.47,0.7)	(0.03,0.91)	(0.01,0.3)	(0.63,0.59)
$\sigma_\alpha \mathcal{R}(s,\sigma)$	$(s_{\sigma_{\alpha,az}}, \sigma_{\sigma_{\alpha,az}})$	(1.94,1.46)	(0,0)	(2.54,0.57)	(0.28,3.14)	(3,0.92)	(1.94,1.46)
	$(s_{\sigma_{\alpha,el}}, \sigma_{\sigma_{\alpha,el}})$	(2.73,2,43)	(0,0)	(4.21,1.05)	(2.74,0.84)	(4.38,1.03)	(2.73,2,43)
$RL \sim \mathcal{R}(s,\sigma)$	(s_{RL}, σ_{RL})	(9.95,1.24)	(7.26,2.55)	(0.06,1.31)	(0.46,6)	(15.43,3.43)	(9.95,1.24)
	μ_{RL}	10	7.77	1.64	7.53	15.82	10

TABLE 2. Parking lot NIST material library.

		Building B2	Building C	Building D1	Building D2	Left and bottom car	Bottom car
$K_{dB} \sim \mathcal{R}(s,\sigma)$	$(s_{K_{pre}}, \sigma_{Kpre})$	(0.18,2.89)	(1.28,9.21)	(3.23,0.72)	(1.48,3.43)	(6.04,1.98)	(0.63,4.79)
	$(s_{K_{post}}, \sigma_{K_{post}})$	(0.13,2.67)	(1.35,2.11)	(2.43,1.23)	(0.13,1.87)	(0.08,1.54)	(0.27,1.87)
$\gamma \sim \mathcal{R}(s,\sigma)$	$(s_{\gamma_{pre}}, \sigma_{\gamma_{pre}})$	(0.54,13.7)	(0.37,8.18)	(7.22,2.38)	(0.92,16.3)	(14.48,3.31)	(0.62,9.71)
	$(s_{\gamma_{post}}, \sigma_{\gamma_{post}})$	(1.02,22.4)	(5.62,34.6)	(34.11,7.9)	(1.03,12.8)	(1.52,15.53)	(10.6,3.48)
$\sigma_s \sim \mathcal{R}(s,\sigma)$	$(s_{\sigma_{spre}}, \sigma_{\sigma_{spre}})$	(0.37,0.23)	(0.05,0.58)	(1.45,0.36)	(0.71,0.25)	(0.65,0.26)	(0.85,0.24)
	$(s_{\sigma_{spost}}, \sigma_{\sigma_{spost}})$	(0.61,0.29)	(0.54,0.1)	(0.84,0.11)	(0.6,0.15)	(0.49,0.21)	(0.78,0.22)
$\lambda \sim \mathcal{R}(s,\sigma)$	$(s_{\lambda_{pre}}, \sigma_{\lambda_{pre}})$	(0,0.2)	(0,0.25)	(0.33,0.06)	(0.08,0.04)	(0,0.14)	(0.1,0.05)
	$(s_{\lambda_{post}}, \sigma_{\lambda_{post}})$	(0.05,0.04)	(0.12,0.06)	(0.3,0.07)	(0.07,0.08)	(0.06,0.04)	(0.16,0.06)
$\sigma_\alpha \mathcal{R}(s,\sigma)$	$(s_{\sigma_{\alpha,az}}, \sigma_{\sigma_{\alpha,az}})$	(6.81,2.12)	(6.24,2.15)	(7.38,0.91)	(4.61,0.68)	(3.16,6.94)	(9.68,4.83)
	$(s_{\sigma_{\alpha,el}}, \sigma_{\sigma_{\alpha,el}})$	(2.18,0.57)	(3.11,1.96)	(2.5,0.82)	(1.89,0.54)	(0.38,3.81)	(4,1.3)
$RL \sim \mathcal{R}(s,\sigma)$	(s_{RL}, σ_{RL})	(18.9,1.9)	(12.5,3.6)	(7.04,1.59)	(21.5,1.92)	(21.4,1.93)	(20.1,4.5)
	μ_{RL}	19.02	13.04	7.22	21.57	21.49	20.56

A computer-aided design (CAD) model of the environment scenario is used as an input to the RT which extracts the geometrical features of a given environment from CAD. These features are represented as several triangles. The RT selects the permutations of triangles combinations to generate the specular components. The indoor and outdoor environment scenarios namely, data center and parking Lot, with 60 GHz and 28 GHz carrier frequency are used.

As shown in Fig. 2a, the data center environment scenario is constructed based on [30], where the room dimension and rack heights are 18 m×18 m×2.56 m and 1.96 m and 2 m, respectively. It is essential to note that this scenario is one of the 802.11 ay use cases where the transmitter and the receiver are supposed to be static and are placed on the rack-tops to have inter-rack connectivity in the case of the Ethernet wired disconnection. The transmitter and the receiver position on the rack-tops are at [8.39, 15.4, 2.19] and [7.92, 4.4, 2.19], respectively.

Any reflected components diffused from the rack sides because one side is loaded with thick cables and server equipment and other side meshed doors at other side. As a result, the rack-sides have higher mean reflection loss $\mu_{RL} = 15.82$ and larger decay constant because of their extended scattering plane and roughness. The walls and columns are covered with drywall, so they have the same reflection loss $\mu RL = 7.35$ dB.

Fig. 2b shows the outdoor scenario of parking Lot which is surrounded by number of buildings. The transmitter is placed at fixed position with respect to the receiver on a building with a height of 2.5 m. the receiver is supposed to be dynamic with 61 different positions. The CAD model for measurement campaign in [13] is generated by using Open Street Map (OSM). The mean (s) and variance (σ) values for Rician, Normal and exponential distributions are obtained using the NIST channel measurements [30] and are considered in material library as shown in Table 1 and 2 for data center and parking Lot environments, respectively. Based on

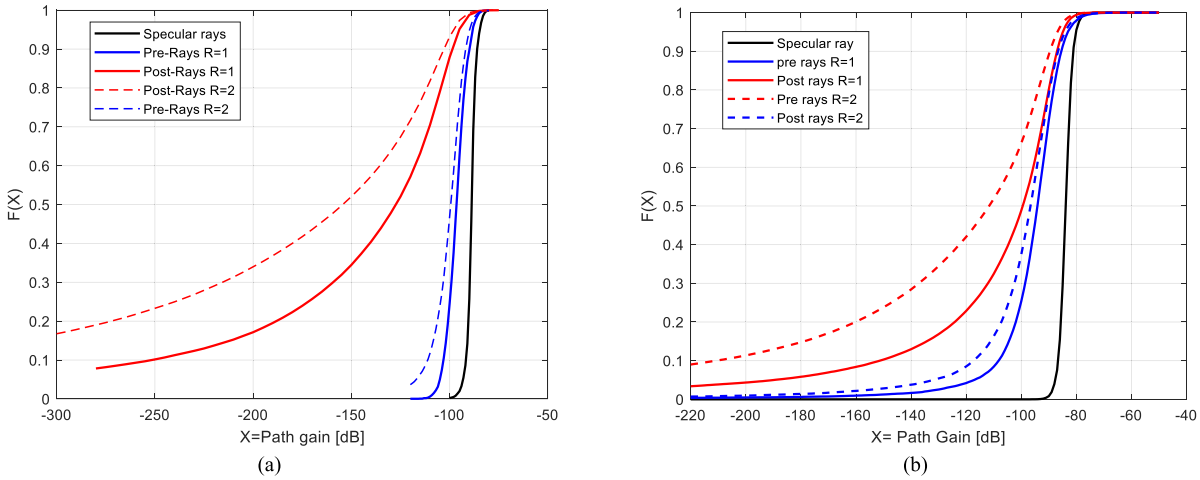

FIGURE 3. Path gains cumulative distribution function for diffuse and specular components (a) data center, (b) parking Lot.

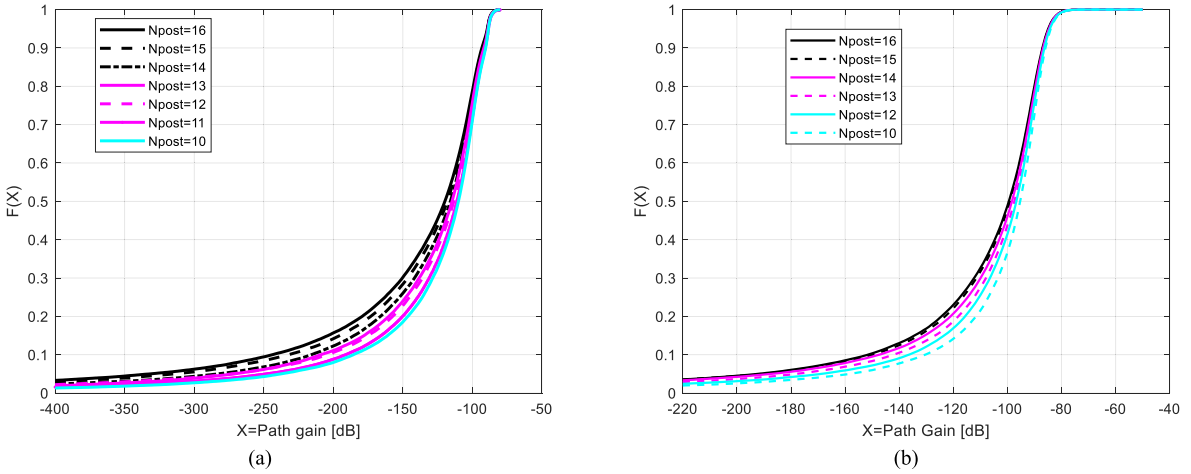

FIGURE 4. Path gains cumulative distribution function of postcursor rays at R=1 (a) data center, (b) parking Lot.

a real channel experiment evidence the number of precursor rays N_{pre}=3 and the number of postcursor rays Npost=16 for the first order reflection (R=1). In the second order reflection (R=2) the Npre/post is doubled.

From (6) and (7) we find that the path gains of diffuse components are based on parameters like K, γ, τ, and S, and all these parameters are randomly generated using different distributions. Consequently, the diffuse component path gains values are also random and varied each time we calculate them. So, we use a cumulative distribution function (CDF) that gives the probability of path gain (PG) will take a value less than or equal to the PG value. Fig. 3 shows the CDF of PG for precursor, postcursor, and specular rays in the case of R=1 and R=2 at data center and parking Lot scenarios. It is obvious that the weakest PG values always result from the postcursor rays either for R=1 or R=2. While the strongest PG values always are caused by the specular rays. In case of data center, Fig. 3a, at CDF=0.5 when R=1, the PG of the postcursor rays is less than the precursor and specular rays by 29 dB and 36 dB, respectively. for R=2 the postcursor PG reduction amount compared to the precursor and specular rays are increased to 50 dB, and 66 dB. When parking lot is considered, Fig. 3b, the PG of post cursor rays, at R=1, is less than the precursor and specular rays by 13 dB and 27 dB, respectively. For R=2 the postcursor PG reduction amount compared to the precursor and specular rays are increased to 39 dB, and 53 dB.

Consequently, the first step to reduce the MPCs numbers by removing the weakest MPCs is to reduce the MPCs that are generated due to postcursor rays. There are two methods to perform this reduction the first method is the reduced post Rays (RPR), and the second method is removed surfaces post rays (RSPR).

A. THE REDUCED POST RAYS (RPR) METHOD

As we mentioned in (3), the total number of MPCs that are generated for each cluster depends on the number of precursor rays and postcursor rays. For A channel model that

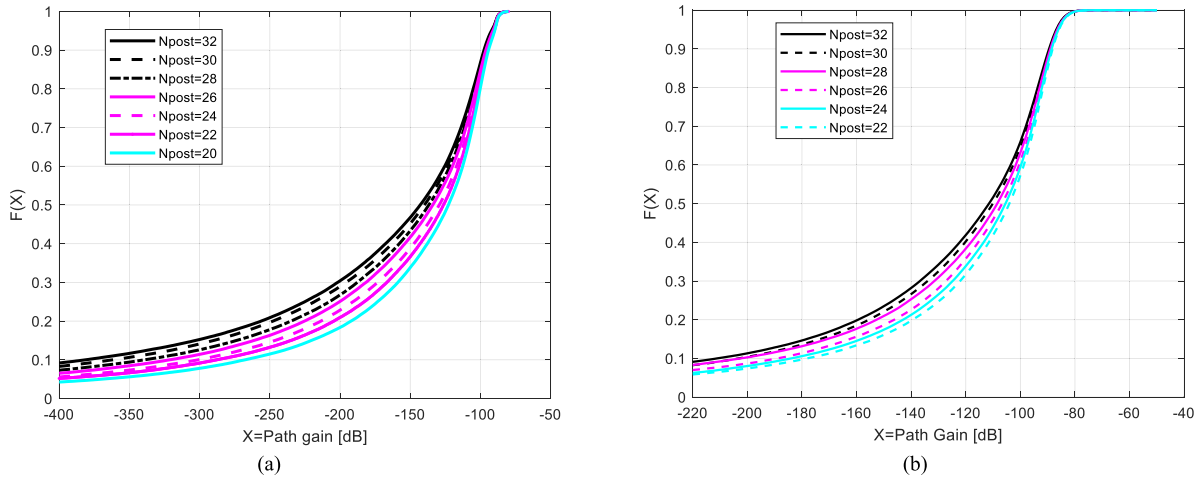

FIGURE 5. Path gains cumulative distribution function of postcursor rays at R=2 (a) data center, (b) parking Lot.

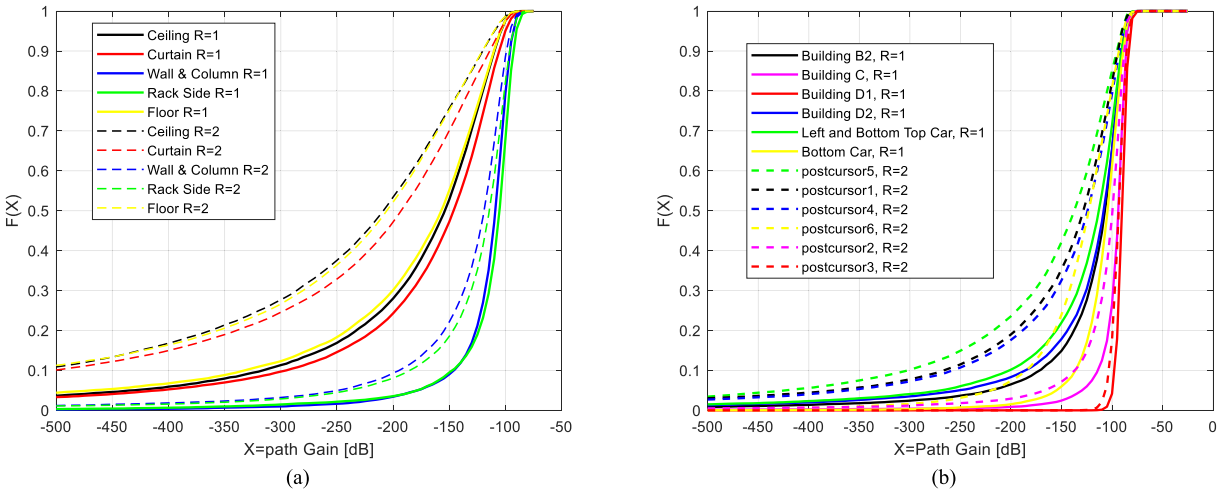

FIGURE 6. Path gains cumulative distribution function of postcursor rays at each surface of data center scenario (a) data center, (b) parking Lot.

based on real measurements, the number of postcursor rays is always greater than the number of precursor rays by nearly five times [28], [30]. Moreover, the weakest path gains of the generated MPCs are belonging to the postcursor rays. As a result, reducing the Npost will help in reducing the number of MPCs and at the same time keep the total signal strength at the receiver nearly unchanged. Figs. 4 and 5 demonstrate the path gains of postcursor rays only at R=1 and R=2, respectively, in a different number of reduced Npost. This is intended to determine the optimum reduced Npost that can achieve the MPCs reduction without losing channel model accuracy. At data center as shown in Fig. 4a, when CDF of 0.3 is considered, the PG is nearly −150 dB at Npost = 16, 15 and 14 while −120 dB at Npost = 10 and 11. When parking Lot is considered, Fig. 4b, the PG is nearly −112 dB at Npost = 16, 15, and 14 while −104 dB at Npost = 10. When R=2, as depicted in Fig. 5a (data center scenario), when CDF of 0.3 is considered, the PG is nearly −200 dB at Npost = 32 and 30 while it is −155 dB and −170 at Npost = 20 and 22, respectively. As it is shown in Fig. 5b, parking Lot scenario, the PG is nearly −200 dB at Npost = 32 and 30 while it is −137 dB and −121 at Npost = 20 and 22, respectively. It is obvious from Fig. 4 and Fig. 5 that as the reduced Npost increase, the postcursor path gains increase but also the difference between the real Npost and the reduced Npost increase, and this will change the channel model accuracy. Determining which several reduced Npost will be used in this method to reduce MPCs depends mainly on the channelmodel accuracy. As it will be demonstrated in the next section, performance evaluation, the optimum reduced Npost will be 14 and 30 postcursor rays for R=1 and R=2, respectively.

B. REMOVED SURFACES POST RAYS (RSPR)METHOD

The postcursor rays are produced subsequent to the specular ray's reflection on a surface in the transmission environment

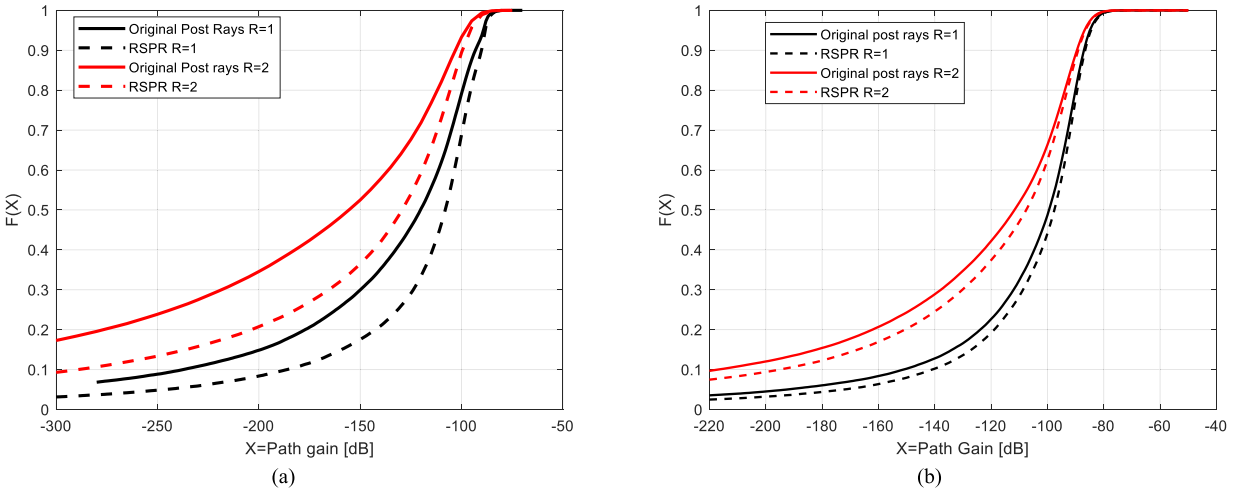

FIGURE 7. Path gains cumulative distribution function of postcursor rays (a) data center after removing ceiling and floor., (b) parking Lot after removing left and bottom car.

situation. This approach involves determining the path gains of the postcursor rays on each surface. The surfaces with the lowest path gains will be eliminated from the QD channel model for post rays exclusively, while precursor rays will still be considered.

As shown in Table 1, only six surfaces participate in generating postcursor rays namely, ceiling, rack-top, curtain, wall and column, rack-side, and floor.

Fig. 6 depicts the post rays' path gains for each surface at R=1 and R=2 at data center and parking Lot scenarios. From Fig. 6a, it is obvious that the ceiling and floor surfaces are responsible for the generation of the weakest path gains in the QD channel model. When CDF=0.5, the path gains that are generated at the ceiling and floorequal to −150 dB and −210 dB for R=1 and R=2.

From Fig. 6b, it is clear that left and bottom top car has the weakest PG. When CDF=0.5, the path gains that are generated at bottom and top car equals to −115 dB and −135 dB for R=1 and R=2, respectively. Therefore, removing these surfaces from the QD channel model will lead to a great amount in MPCs reduction without affecting the channel model accuracy as it will be shown later.

Fig. 7a shows the CDF path gains of the postcursor rays before and after removing ceiling and floor surfaces at data center scenario. the post rays' path gains after removing surfaces when CDF of 0.5 is considered are increased by 13 dB and 25 dB at R=1 and R=2, respectively. Fig. 7b shows the CDF PG of the postcursor rays before and after removing left and bottom top car at parking Lot scenario. the post rays' path gains after removing surfaces when CDF of 0.5 is considered are increased by 13 dB and 15 dB at R=1 and R=2, respectively.

IV. PERFORMANCE EVALUATION RESULTS

This section assesses the effectiveness of the proposed techniques using two fundamental measures: computational reduction and accuracy. The computational reduction achieved by applying the reduction methods is evaluated based on computational time and complexity. Additionally, we evaluate the impact of this reduction on the accuracy of the QD channel model, considering factors such as:

1) path gain CDF: we use this metric instead of the double directional channel impulse response (DDIR) as the latter is randomly generated and has a different result each time the simulator runs.
2) SNR: it is used to show the accuracy level of the QD channel model at the link layer.
3) Intra-cluster statistics namely, K-factor, power delay decay, delay spread, and azimuth angular spread.

A. COMPUTATIONAL PERFORMANCE

The MPCs reduction percentage for the RPR and the RSPR methods. It is defined as:

$$N_{MPC-reduction}\% = \frac{N - N'}{N} X100 \tag{11}$$

where N' is the number of reduced MPCs. It is obvious from table 2, that the RPR method can achieve a greater MPCs reduction amount by increasing the number of reduced N_{post}. However, this increment in MPC reduction amount affects the QD channel model accuracy as it will be explained in the next subsection B. The RSPR method attains a higher MPCs reduction percentage than that attained by the RPR method when N_{post} =14 is considered. Moreover, the reflection order has a slight impact on the MPCs reduction amount in the case of RPR and RSPR methods. The steps that illustrate the proposed simplified methods are shown in algorithm 1.

The main purpose of reducing MPCs is to minimize the computational time required by the simulator that realizes the QD channel model and consequently reduces the model complexity.

Algorithm 1 Proposed MPCs Reduction Algorithm

inputs($PG_{0,dB}$, τ_0, Npost, material library)
Calculate $PG_{pre,dB}$
Calculate $PG_{post,dB}$
If ($PG_{post,dB}$ <$PG_{pre,dB}$)
%RSPR Method
ForR=1: n %n=number of surfaces
Calculate Path gain for each surface in environment scenario ($PG_{post,R,dB}$)
If ($PG_{post,R,dB}$ ==min($PG_{post,R,dB}$(R)))
$PG_{post,dB}$ =sum($PG_{post,R,dB}$(R))- $PG_{post,R,dB}$
Else
End
End
%RPR Method
Fori=1: Npost
Calculate$PG_{post,dB}$ at Npost
Calculate$PG_{post,dB}$ at (Npost-i)
Γ=$PG_{post,dB}$ at Npost- $PG_{post,dB}$ at (Npost-i)
If (Γ ≈**zero)**
$PG_{post,dB}$ = $PG_{post,dB}$ at (Npost-i)
else
End
End

TABLE 3. The proposed methods MPC reduction percentage comparison.

	R	(RSPR)	(RPR)	
MPCs Reduction	R =1	16.6%	10% (N_{post}=14)	30% (N_{post}=10)
	R =2	15%	10% (N_{post}=28)	32% (N_{post}=22)
Computational Time	R=1	17%	13.3%	33.3%
	R=2	14%	9%	29.5%

According to [32] Computational Time is given by:

$$T = \left[\left(\frac{2\pi}{\text{AoDAZ}} X \frac{\pi}{\text{AoDEL}}\right) + (N_{MPC})\right] Xt \tag{12}$$

where: AoDAZ, AoDEL, N_{MPC}, and t are the average azimuth angle of departure, the average elevation angle of departure, the total number of MPCs, and the average simulation time for each ray.

It is obvious from Table 3 that utilizing RPR and RSPR methods succeed in saving the computational time of the QD channel model simulator. However, the amount of computational time saving is decreased at higher reflection order (R=2) in the two proposed methods. The RSPR method achieves a computational time reduction than that achieved by the RPR method when N_{post} =14 is considered.

According to [24], the RT complexity is denoted by:

$$\mathcal{C} = RT^{R+1} \tag{13}$$

where T is the number of extracted triangles from CAD and R is the reflection order. The two proposed methods remove $(N - N')$ rays. This means that for every ray of reflection order R, none of the (R+1)T operations are performed if the ray is discarded [24]. Consequently, the computational complexity in (13) will be:

$$\mathcal{C} = RT^{R} \tag{14}$$

As a result, the RT complexity is reduced by factor T which equals 360 triangles for the Data Center scenario.

B. QD CHANNEL MODEL ACCURACY

1) PATH GAIN

Fig. 8 compares the path gain CDF of the QD channel model in different numbers of post rays. The original QD model without using RPR is at N_{post} =16 and 32. The solid lines and dash lines in Fig. 8 indicate using the RPR method at R=1 and R=2, respectively. It is obvious that as the reduced N_{post} increase the difference between the QD channel model with and without utilizing RPR becomes greater. For example, when CDF 0f 0.3 is considered, at Fig. 8a, the difference is about 5 dB and 10 dB at Npost=14 and 28, respectively, and is about 20 dB and 40 dB at Npost=10 and 20, respectively. At parking Lot scenario, Fig. 8b, the difference is about 2 dB and 5 dB at Npost =14 and 28, respectively, and is about 6 dB and 15 dB at Npost=10 and 20, respectively. This means that the original QD channel model is changed. When N_{post} = 14 and 28 for R=1 and R=2, respectively, the simplified QD channel model is closer to the original model and attains an acceptable MPCs reduction percentage of 10%.

Regarding the RSPR method, it is clear from Fig. 9a that removing the post rays resulting from the ceiling and floor surfaces helps in increasing the QD path gains compared to the path gains of the original QD channel model in case of data center scenario and when parking Lot is considered, discarding left and bottom car increases the original QD PG. However, this leads to a greater difference between the original QD and RSPR compared to the RPR method. When the CDF>0.5 is considered, this difference becomes smaller.

2) SNR

The channel matrix between transmitter and receiver is given by:

$$H_{tx,rx} = \sum_{n=1}^{N} \sqrt{\text{PG}_\text{N}} e^{j(-2\pi\tau_m f_c)} a_{rx}^{*}(\text{AOA}_\text{n}) a_{tx}^{H}(\text{AOD}_\text{n}) \tag{15}$$

where fc is the carrier frequency which equals to 60GHz and 28 GHz at data center and parking Lot scenarios, respectively, $a_{rx}^{*}(AOA_n)$, $a_{tx}^{H}(AOD_n)$ are the angle array response at receiver and transmitter, respectively. a^* is the conjugate operator and a^H is the Hermitian operator. Denote received signal power and noise power by $P_{tx}$and P_n, respectively. The SNR after optimal beamforming is given as by:

$$\text{SNR} = \frac{P_{tx} H_{tx,rx}}{P_n} \tag{16}$$

Fig. 10 and Fig. 11 depict the effect of applying RPR and RSPR methods on the SNR of the QD channel model at

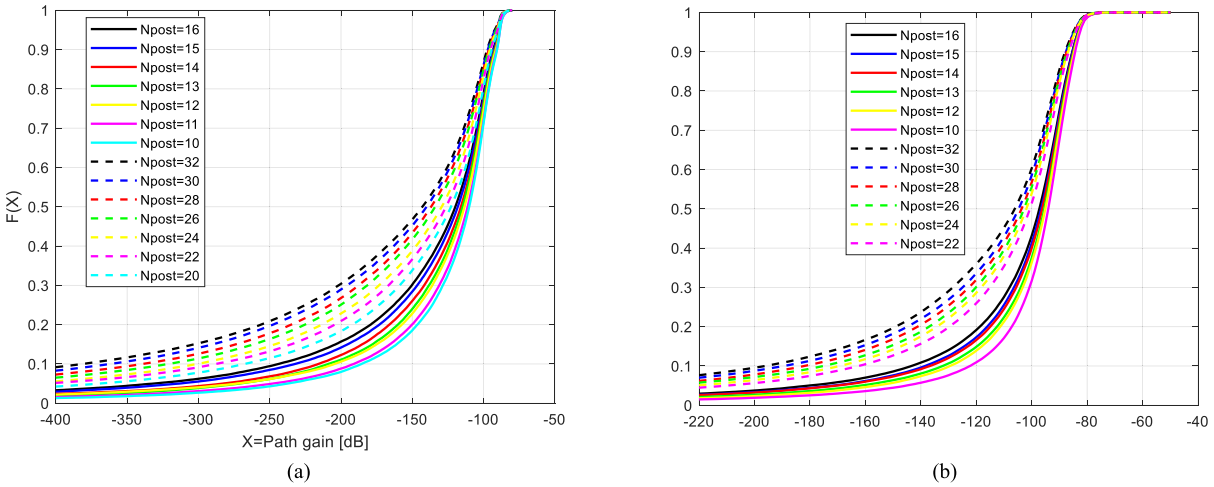

FIGURE 8. Path gains cumulative distribution function of QD channel model at RPR method a) data center, (b) parking Lot.

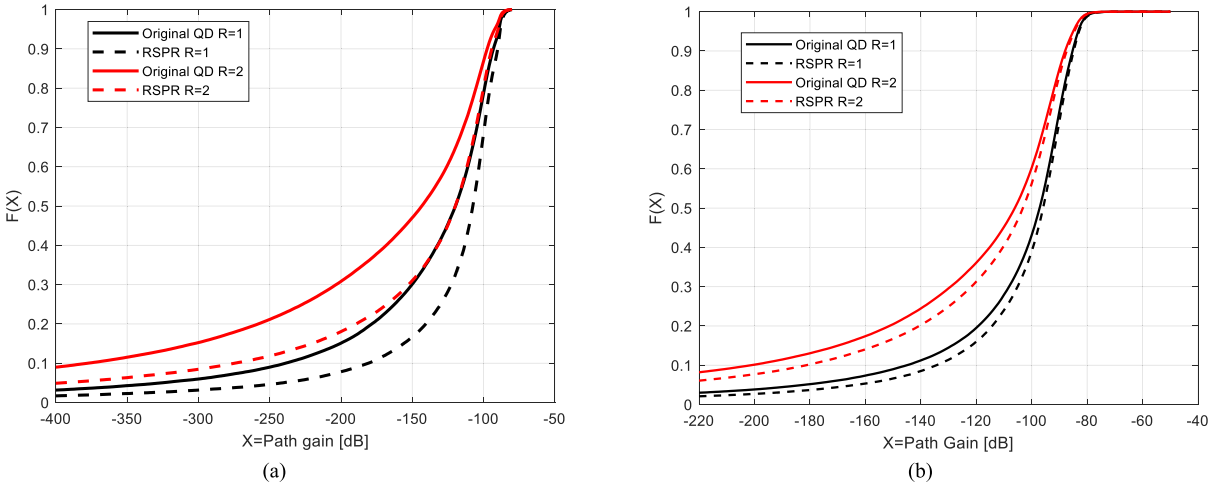

FIGURE 9. Path gains cumulative distribution function of QD channel model at RSPR method a) data center, (b) parking Lot.

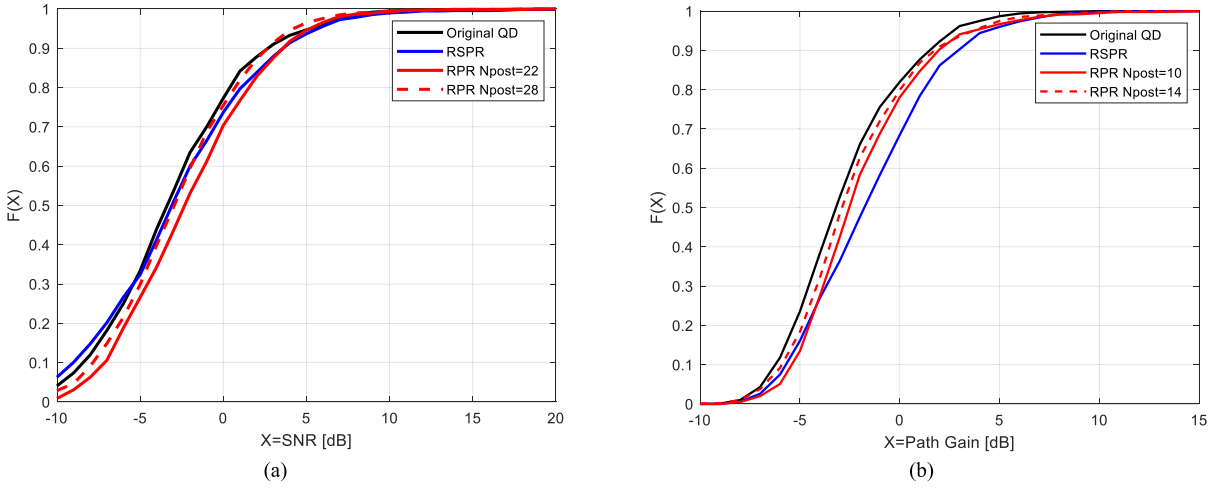

FIGURE 10. Signal to noise ratio cumulative distribution function at R=1 a) data center, (b) parking Lot.

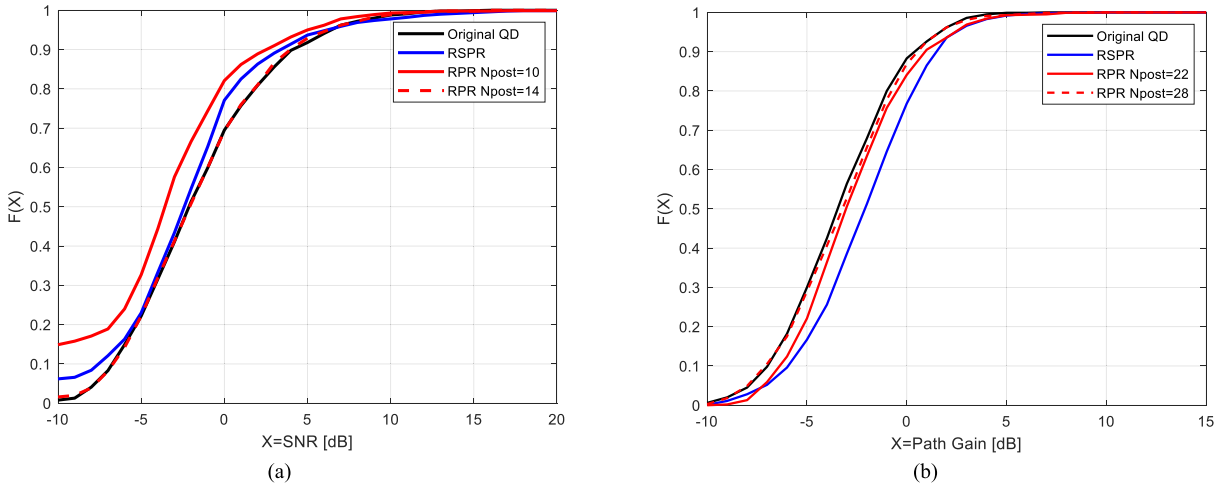

FIGURE 11. Signal to noise ratio cumulative distribution function at R=2 a) data center, (b) parking Lot.

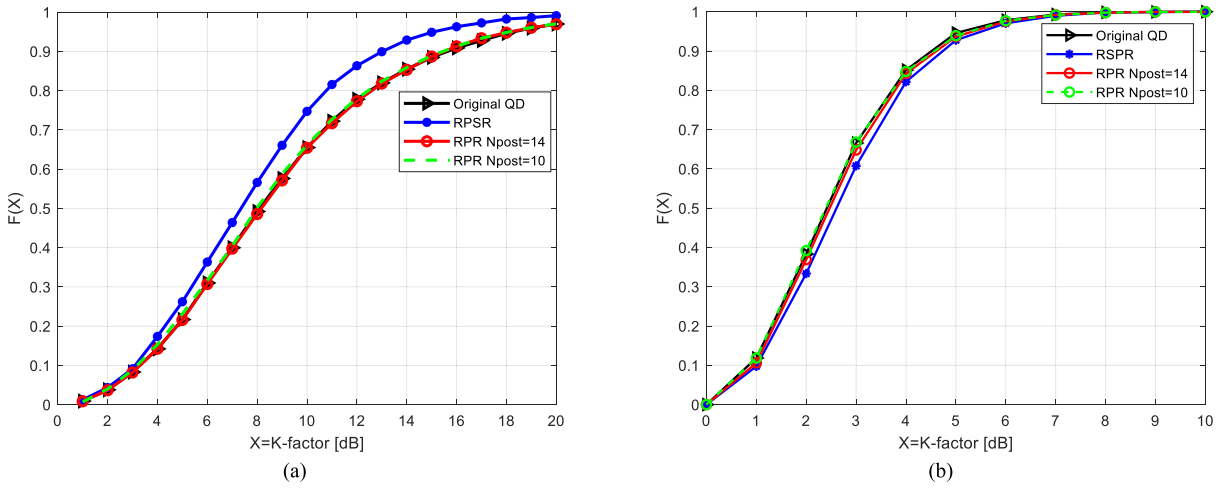

FIGURE 12. Intra cluster K-factor cumulative distribution function a) data center, (b) parking Lot.

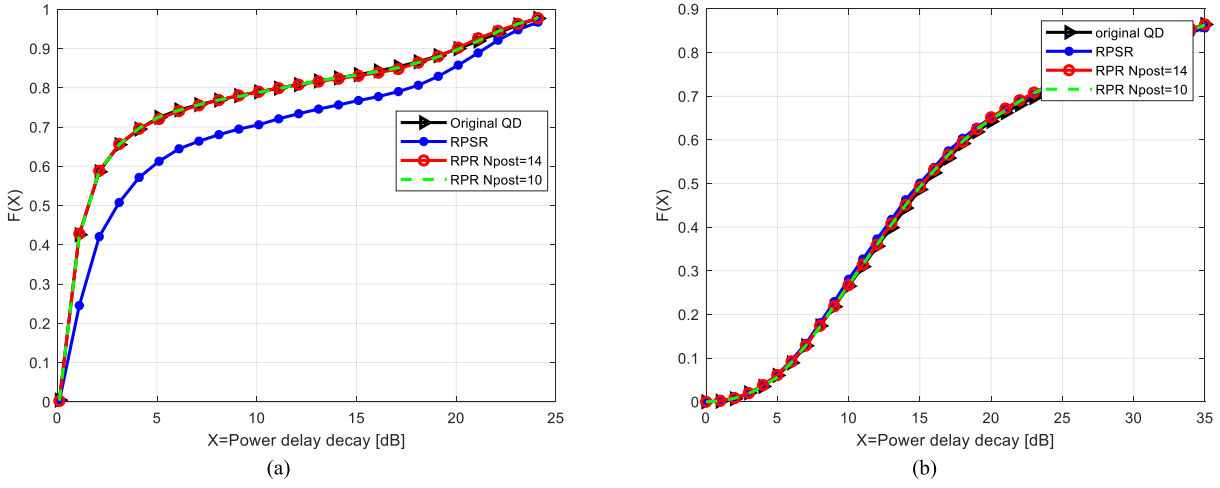

FIGURE 13. Intra cluster power delay decay cumulative distribution function a) data center, (b) parking Lot.

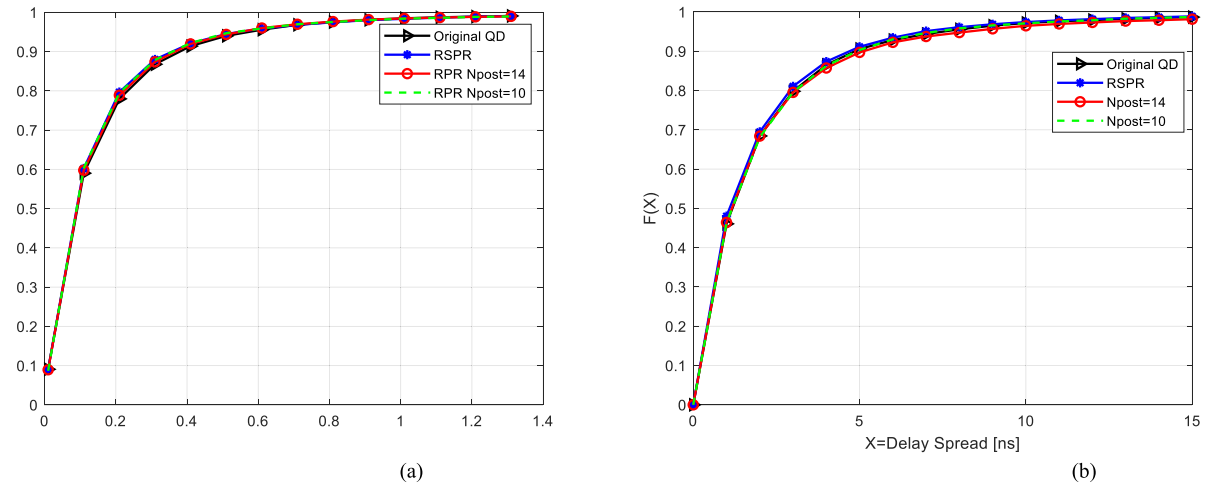

FIGURE 14. Intra cluster delay spread cumulative distribution function a) data center, (b) parking Lot.

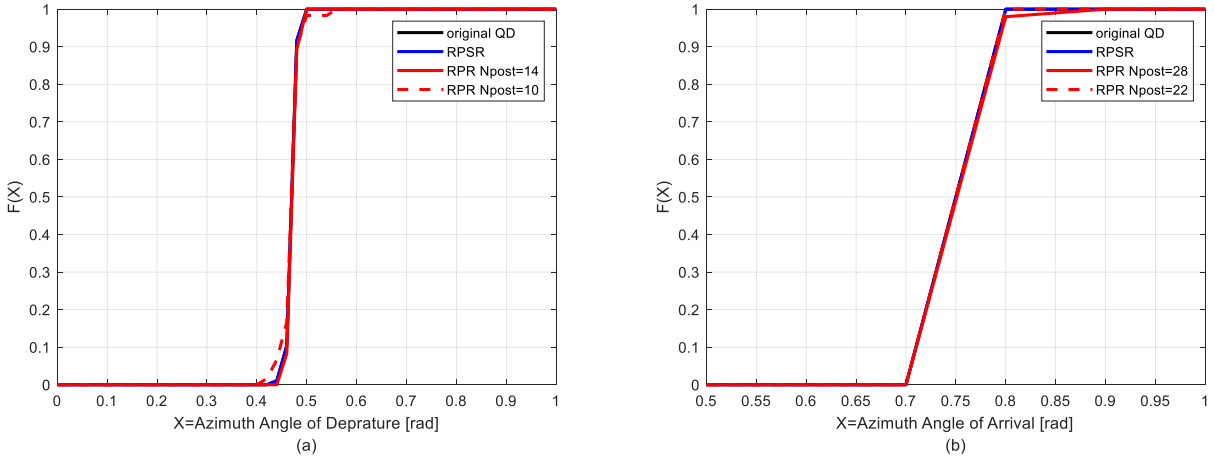

FIGURE 15. Intra cluster angular spread cumulative distribution function of data center (a) Azimuth AoD, (b) Azimuth AoA.

R=1 and R=2, respectively, when data center and parking Lot scenarios are considered. The transmitted power (P_{tx} is assumed to be 30 dBm as in [24]. It is obvious that using the two simplification methods changes the QD SNR performance but with minimal change. For R=1, as shown in Fig. 10a, when data center scenario is used, utilizing the RPR method with Npost=14, the QD SNR is the same as that of the original QD while with N_{post}=10, the SNR difference becomes 2 dB at CDF=0.5. In the case of the RSPR method, the QD SNR is slightly changed from the original QD. When parking Lot is mentioned, the RPR method with Npost=14, the QD SNR is nearly the same as that of the original QD but with N_{post}=10, the SNR difference becomes 1 dB at CDF=0.5. In the case of the RSPR, the QD SNR is changed from the original QD by 2 dB.

For R=2, as shown in Fig. 11a, the QD SNR of RSPR and RPR with N_{post}=28 performances are the same and are slightly different from the original QD when Npost=22.

For parking Lot, Fig. 11b, the QD SNR of RPR with performances is nearly the same as the of original QD. And it is slightly different from the original QD by 1 dB, when RSPR method is used.

3) INTRA-CLUSTER STATISTICS

It is particularly important, after reducing the multipath, to make sure that the intra-cluster statistics are not changed. Fig. 12 to 15 depict the comparison between the intra-cluster statistics of K-factor, power delay decay, delay spread, and azimuth angular spread, respectively, before and after the multipath reduction methods when data center and parking Lot scenarios are applied. The number of reflections has an impact on intra-cluster statistics. However, the accuracy performance of intra-cluster statistics at second reflection order is attained as in first reflection order. So, the presented intra-cluster statistics in this paper are investigated at first order reflection.

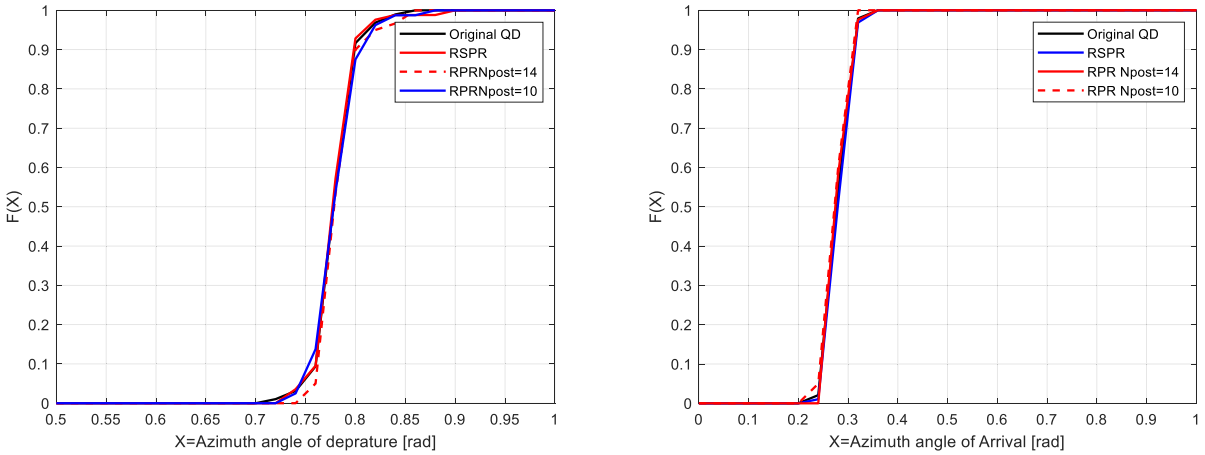

FIGURE 16. Intra cluster angular spread cumulative distribution function of parking lot (a) Azimuth AoD, (b) Azimuth AoA.

TABLE 4. Comparison for different simplified mmwave channel model methods.

Simplified Channel Model methods	Computational time reduction %	Accuracy evaluation	Accuracy Performance
Simplified SCM 3GPP [27]	10%	SNR, LCR, AFBW, MSVR	Consistent
Simplified RT [24]	11%	SNR, throughput	Consistent
Proposed RSPR	17%	PG, SNR, Intra-cluster statistics	Consistent
Proposed RPR	13%		

TABLE 5. RPR and RSPR tradeoff comparison.

	Complexity compared to original QD			Accuracy compared to original QD	
	MPCs reduction	**Computational time reduction**	**Complexity**	**SNR**	**Intra-cluster statistics**
RPR	lower	lower	RT^R	Totally agreement at Npost=14 &28	Totally agreement
RSPR	higher	higher	RT^R	Totally agreement at indoor scenario Partially agreement at outdoor scenario	partially agreement

Fig. 12 to 15 it is depicted that removing the weakest paths using the RPR method keeps all intra-cluster statistics consistent. However, utilizing the RSPR method had a lower agreement with the original QD channel model because there are two whole entire surfaces which are completely removed. As a result, the cluster statistics will change. When CDF=0.5 the RSPR differs by 1 dB and 2 dB in the case of intra-cluster K-factor and power delay decay as in Fig. 12a and 13a, respectively. In Fig. 12b and 13b, the RSPR method show higher agreement with the original QD as there is one surface that is neglected from the environment.

On other hand, RSPR has a good agreement in case of delay and azimuth angular spread at both data center and parking Lot scenarios as shown in Fig. 15 and Fig. 16. This is because the cluster numbers are not changed when the RPR method is applied and are reduced when RSPR is applied, and the cluster numbers have no correlation with delay and angular spread and have a weak correlation with K-factor and power decay [33].

V. COMPLEXITY AND ACCURACY TRADE OFF COMPARISON

We present in table 4, a comparison for computational time, and accuracy comparison for the proposed simplified methods and the simplified methods in literature, namely, simplified SCM 3GPP [27] method and simplified ray tracer (RT) method [24]. In SCM 3GPP method, the simplification is attained by reducing the number of clusters and spatial components of the channel. In simplified RT method, the weakest MPCs is discarded based on how low their path gain is compared to the strongest MPC. Table 5 shows the comparison between the proposed methods and other methods in terms of computational reduction percentage and accuracy performance. The results of the proposed methods in table 4 are at the first order of reflection (R=1) and at Npost=14 in case of RPR method. Compared to simplified SCM 3GPP method, the proposed methods achieve higher computational time reduction by 4% and 0.5% in case of RSPR and RPR, respectively. The proposed methods attain

higher reduction amount of computational time by 5% and 2% at RSPR and RPR, respectively. The accuracy of simplified SCM 3GPP method was evaluated in terms of SNR, level crossing frequency (LCF), average fading band width (AFBW), and mean singular value ratio of channel (MSVR) and was evaluated in terms of SNR and throughput in case of simplified RT method and was evaluated in terms of SNR and intra-cluster statistics in case of proposed methods. All methods show consistent accuracy compared to the baseline model before simplification.

For the purpose of using RT efficiently, the comparison between RPR and RSPR methodsis summarized in Table 5 compared to original QD model. It is obvious that the RSPR outperformance the RPR, only in computational time reduction and total MPCs reduction amount when N=14 and N=28 at first and second reflection order, respectively. However, this is attained at the price of a slight change in intra-cluster statistics, namely K-factor and power delay decay. The RPR can be updated to achieve more computational time reduction than RSPR by using a number of post rays less than 14 and 28 at the first and second order of reflection. Nevertheless, this would cost a minimum change in SNR. The intra-cluster statistics delay spread and angular spread of RPR and RSPR have total agreement with the statistics of the original QD model. Moreover, the complexity reduction amount in the two methods is the same.

VI. CONCLUSION

Developing an accurate and scalable simulator for simplified mmWave QD channel models is essential for future wireless communication. In this paper, we proposed two methods for reducing the generated MPCs by removing the MPCs with the weakest path gains. The first method is RSPR which discards the reflected surfaces that introduce the weakest path gains. The second method is RPR which reduces the number of post rays as it was the cause of the weakest path gains. We evaluated the impact of these methods on computational reduction and on channel model accuracy. The analysis and evaluation were applied to real measurement data of indoor environment data center scenario at 60 GHz and outdoor parking lot environment scenario at 28 GHz. Based on the performance evaluation results, it was found that the simplified reduction methods proposed have achieved an ideal trade-off between the reduction in computational time and the accuracy of the QD channel model across different reflection orders. The proposed methods' accuracy and complexity were evaluated using measured data obtained from indoor and outdoor environments operating at 60 GHz and 28 GHz, respectively. The balance between the two variables was demonstrated by testing both first and second-order reflection orders. The simplified methods proposed were found to reduce computational time by around 16% and 11% for RSPR and RPR schemes, respectively, when compared to the original QD.

REFERENCES

[1] H. Zhang, Y. Zhang, J. Cosmas, and N. Jawad, "MmWave indoor channel measurement campaign for 5G new radio indoor broadcasting," *IEEE Trans. Broadcast.*, vol. 68, no. 2, pp. 331–344, Jun. 2022, doi: 10.1109/TBC.2021.3131864.

[2] S. H. R. Naqvi, P. H. Ho, and L. Peng, "5G NR mmWave indoor coverage with massive antenna system," *J. Commun. Netw.*, vol. 23, no. 1, pp. 1–11, Feb. 2021, doi: 10.23919/JCN.2020.000031.

[3] M. E. Diago-Mosquera, A. Aragon-Zavala, and M. Rodriguez, "Towards practical path loss predictions in indoor corridors considering 5G mmWave three-dimensional measurements," *IEEE Antennas Wireless Propag. Lett.*, vol. 21, no. 10, pp. 2055–2059, Oct. 2022, doi: 10.1109/LAWP.2022.3190324.

[4] C. X. Wang, J. Huang, H. Wang, X. Gao, X. You, and Y. Hao, "6G wireless channel measurements and models: Trends and challenges," *IEEE Veh. Technol. Mag.*, vol. 15, no. 4, pp. 22–32, Dec. 2020, doi: 10.1109/MVT.2020.3018436.

[5] W. Hong, Z. H. Jiang, C. Yu, D. Hou, H. Wang, C. Guo, Y. L. Hu Kuai, Y. Yu, Z. Jiang, Z. Chen, J. Chen, Z. Yu, J. Zhai, N. Zhang, L. Tian, F. Wu, G. Yang, Z.-C. Hao, and J. Y. Zhou, "The role of millimeter-wave technologies in 5G/6G wireless communications," *IEEE J. Microw.*, vol. 1, no. 1, pp. 101–122, Jan. 2021, doi: 10.1109/JMW.2020.3035541.

[6] A. V. Lopez, A. Chervyakov, G. Chance, S. Verma, and Y. Tang, "Opportunities and challenges of mmWave NR," *IEEE Wireless Commun.*, vol. 26, no. 2, pp. 4–6, Apr. 2019, doi: 10.1109/MWC.2019.8700132.

[7] S. Niknam, B. Natarajan, and R. Barazideh, "Interference analysis for finite-area 5G mmWave networks considering blockage effect," *IEEE Access*, vol. 6, pp. 23470–23479, 2018, doi: 10.1109/ACCESS.2018.2829621.

[8] L. Zhu, S. Wang, and J. Zhu, "Adaptive beamforming design for millimeter-wave line-of-sight MIMO channel," *IEEE Commun. Lett.*, vol. 23, no. 11, pp. 2095–2098, Nov. 2019, doi: 10.1109/lcomm.2019.2936379.

[9] Q. Abdullah et al., "Maximising system throughput in wireless powered sub-6 GHz and millimetre-wave 5G heterogeneous networks," *Telkomnika*, vol. 18, no. 3, p. 1185, Jun. 2020, doi: 10.12928/telkomnika.

[10] A. Salh, L. Audah, Q. Abdullah, O. Aydogdu, M. A. Alhartomi, S. H. Alsamhi, F. A. Almalki, and N. S. M. Shah, "Low computational complexity for optimizing energy efficiency in mm-wave hybrid precoding system for 5G," *IEEE Access*, vol. 10, pp. 4714–4727, 2022, doi: 10.1109/ACCESS.2021.3139338.

[11] A. Salh, L. Audah, N. S. Mohd Shah, and S. Anuar Hamzah, "Energy-efficient power allocation with hybrid beamforming for millimetre-wave 5G massive MIMO system," *Wireless Pers. Commun.*, vol. 115, no. 1, pp. 43–59, Jun. 2020, doi: 10.1007/s11277-020-07559-w.

[12] J. Park, S.-L. Kim, and J. Zander, "Tractable resource management with uplink decoupled millimeter-wave overlay in ultra-dense cellular networks," *IEEE Trans. Wireless Commun.*, vol. 15, no. 6, pp. 4362–4379, Jun. 2016, doi: 10.1109/TWC.2016.2540626.

[13] J. G. Andrews, T. Bai, M. Kulkarni, A. Alkhateeb, A. Gupta, and R. W. Heath, "Modeling and analyzing millimeter wave cellular systems," *IEEE Trans. Commun.*, vol. 65, no. 1, pp. 403–430, Jan. 2017, doi: 10.1109/TCOMM.2016.2618794.

[14] P. Ferrand, M. Amara, S. Valentin, and M. Guillaud, "Trends and challenges in wireless channel modeling for evolving radio access," *IEEE Commun. Mag.*, vol. 54, no. 7, pp. 93–99, Jul. 2016, doi: 10.1109/MCOM.2016.7509384.

[15] M. T. Dabiri and M. Hasna, "3D uplink channel modeling of UAV-based mmWave fronthaul links for future small cell networks," *IEEE Trans. Veh. Technol.*, vol. 72, no. 2, pp. 1400–1413, Feb. 2023, doi: 10.1109/TVT.2022.3209988.

[16] S. Zeb, A. Mahmood, S. A. Hassan, M. Gidlund, and M. Guizani, "Analysis of beyond 5G integrated communication and ranging services under indoor 3-D mmWave stochastic channels," *IEEE Trans. Ind. Informat.*, vol. 18, no. 10, pp. 7128–7138, Oct. 2022, doi: 10.1109/TII.2022.3146166.

[17] J. Ghosh, H. Haci, N. Kumar, K. A. Al-Utaibi, S. M. Sait, and C. So-In, "A novel channel model and optimal power control schemes for mobile mmWave two-tier networks," *IEEE Access*, vol. 10, pp. 54445–54458, 2022, doi: 10.1109/ACCESS.2022.3176320.

[18] S. Sun, G. R. MacCartney, and T. S. Rappaport, "A novel millimeter-wave channel simulator and applications for 5G wireless communications," in *Proc. IEEE Int. Conf. Commun. (ICC)*, Paris, France, May 2017, pp. 1–7.

[19] M. R. Akdeniz, Y. Liu, M. K. Samimi, S. Sun, S. Rangan, T. S. Rappaport, and E. Erkip, "Millimeter wave channel modeling and cellular capacity evaluation," *IEEE J. Sel. Areas Commun.*, vol. 32, no. 6, pp. 1164–1179, Jun. 2014, doi: 10.1109/JSAC.2014.2328154.

[20] I. Winner, "WINNER II channel models," Inf. Soc. Technol., Finland, Tech. Rep. IST-4-027756, 2007.

[21] J. Meinilä, P. Kyösti, T. Jämsä, and L. Hentilä, "WINNER II channel models," in *Radio Technologies and Concepts for IMT-Advanced*. Chichester, U.K.: Wiley, 2009, pp. 39–92.

[22] T. Zugno, M. Polese, N. Patriciello, B. Bojović, S. Lagen, and M. Zorzi, "Implementation of a spatial channel model for NS-3," in *Proc. Workshop NS-3*, New York, NY, USA, 2020, pp. 49–56.

[23] M. Lecci, M. Polese, C. Lai, J. Wang, C. Gentile, N. Golmie, and M. Zorzi, "Quasi-deterministic channel model for mmWaves: Mathematical formalization and validation," in *Proc. IEEE Global Commun. Conf. (GLOBECOM)*, Taiwan, Dec. 2020, pp. 1–6.

[24] C. Lai, R. Sun, C. Gentile, P. B. Papazian, J. Wang, and J. Senic, "Methodology for multipath-component tracking in millimeter-wave channel modeling," *IEEE Trans. Antennas Propag.*, vol. 67, no. 3, pp. 1826–1836, Mar. 2019, doi: 10.1109/TAP.2018.2888686.

[25] V. Degli-Esposti, "A diffuse scattering model for urban propagation prediction," *IEEE Trans. Antennas Propag.*, vol. 49, no. 7, pp. 1111–1113, Jul. 2001, doi: 10.1109/8.933491.

[26] R. Charbonnier, C. Lai, and T. Tenoux, "Calibration of ray-tracing with diffuse scattering against 28-GHz directional urban channel measurements," *IEEE Trans. Veh. Technol.*, vol. 69, no. 12, pp. 14264–14276, Dec. 2020, doi: 10.1109/TVT.2020.3038620.

[27] M. Lecci, P. Testolina, M. Polese, M. Giordani, and M. Zorzi, "Accuracy versus complexity for mmWave ray-tracing: A full stack perspective," *IEEE Trans. Wireless Commun.*, vol. 20, no. 12, pp. 7826–7841, Dec. 2021, doi: 10.1109/TWC.2021.3088349.

[28] P. Testolina, M. Lecci, M. Polese, M. Giordani, and M. Zorzi, "Scalable and accurate modeling of the millimeter wave channel," in *Proc. Int. Conf. Comput., Netw. Commun. (ICNC)*, Big Island, HI, USA, Feb. 2020, pp. 969–974.

[29] M. Lecci, P. Testolina, M. Giordani, M. Polese, T. Ropitault, C. Gentile, N. Varshney, A. Bodi, and M. Zorzi, "Simplified ray tracing for the millimeter wave channel: A performance evaluation," in *Proc. Inf. Theory Appl. Workshop (ITA)*, San Diego, CA, USA, Feb. 2020, pp. 1–6.

[30] J. Senic, C. Gentile, P. B. Papazian, K. A. Remley, and J.-K. Choi, "Analysis of E-band path loss and propagation mechanisms in the indoor environment," *IEEE Trans. Antennas Propag.*, vol. 65, no. 12, pp. 6562–6573, Dec. 2017, doi: 10.1109/TAP.2017.2722876.

[31] C. Gentile, P. B. Papazian, R. Sun, J. Senic, and J. Wang, "Quasi-deterministic channel model parameters for a data center at 60 GHz," *IEEE Antennas Wireless Propag. Lett.*, vol. 17, no. 5, pp. 808–812, May 2018, doi: 10.1109/LAWP.2018.2817066.

[32] A. Maltsev, A. Pudeyev, I. Karls, I. Bolotin, G. Morozov, R. Weiler, M. Peter, and W. Keusgen, "Quasi-deterministic approach to mmWave channel modeling in a non-stationary environment," in *Proc. IEEE Globecom Workshops (GC Wkshps)*, Austin, TX, USA, Dec. 2014, pp. 966–971.

[33] F. Hossain, T. Geok, T. Rahman, M. Hindia, K. Dimyati, S. Ahmed, C. Tso, and N. Abd Rahman, "An efficient 3-D ray tracing method: Prediction of indoor radio propagation at 28 GHz in 5G network," *Electronics*, vol. 8, no. 3, p. 286, Mar. 2019, doi: 10.3390/electronics8030286.

[34] Y. Chen, Y. Li, C. Han, Z. Yu, and G. Wang, "Channel measurement and ray-tracing-statistical hybrid modeling for low-terahertz indoor communications," *IEEE Trans. Wireless Commun.*, vol. 20, no. 12, pp. 8163–8176, Dec. 2021, doi: 10.1109/TWC.2021.3090781.

RADWA A. ROSHDY received the B.Sc., M.Sc., and Ph.D. degrees from the Department of Electronics and Communications Engineering, Zagazig University, Zagazig, Egypt, in 2008, 2014, and 2020, respectively. She is currently an Assistant Professor with the Department of Electrical and Computer Engineering, Higher Technological Institute, 10th of Ramadan City. She was a peer reviewer of SCI journals and a conference reviewer and organizer. Her research interests include channel estimation, reconfigurable intelligent surfaces, channel modeling, wireless communications, and the Internet of Things.

MOSTAFA H. DAHSHAN received the B.Sc. degree in computer engineering from Cairo University, Egypt, in 1999, and the M.Sc. degree in telecommunication systems and the Ph.D. degree in electrical and computer engineering from The University of Oklahoma, USA, in 2002 and 2006, respectively. He is currently an Assistant Professor of computer engineering with the College of Computer and Information Sciences, King Saud University, Saudi Arabia. His research interests include network security, wireless sensor networks, the Internet of Things, and network optimization problems.

SALMAN A. ALQAHTANI (Member, IEEE) is currently a Full Professor with the Department of Computer Engineering, College of Computer and Information Sciences, King Saud University, Riyadh, Saudi Arabia. He is also a Senior Consultant in computer communications, integrated solutions, and digital forensics for few development companies and government sectors in Saudi Arabia. His main research interests include radio resource management (RRM) for wireless and cellular networks, such as 4G, 5G, the IoT, Industry 4.0, LTE, LTE advanced, Femtocell, cognitive radio, and cyber sovereignty, with a focus on call admission control (CAC), packet scheduling, radio resource sharing, quality-of-service (QoS) guarantees for data services, performance evaluation of packet-switched networks, system models, simulations and integration of heterogeneous wireless networks, and digital forensics.

AHMED EMAM received the B.Sc. degree from Ain Shams University, Cairo, Egypt, the M.Sc. degree from Menoufia University, Menoufia, Egypt, and the Ph.D. degree from the Department of Computer Science and Computer Engineering, Speed Engineering School, University of Louisville, Louisville, KY, USA, in Summer 2001. From 2001 to 2021, he is currently a Professor of information systems at the College of Computer and Information Systems, King Saud University, where he teaches database systems, data mining, and big data analytics. From 2022, he is currently the Dean of computer science and engineering collage, King Salman International university, Egypt.

HOSSAM M. KASEM received the Ph.D. degree from the Egypt–Japan University of Science and Technology (E-JUST), Egypt, in 2015. From 2015 to 2017, he was an Assistant Professor with the Faculty of Engineering, Tanta University, Egypt. From 2017 to 2019, he has been a Post-Doctoral Fellow with the Research Institute for Future Media Computing, Shenzhen University, China. Since 2019, he is currently an Associate Professor at electronics and electrical communications, faculty of engineering, Tanta university. His research interests include deep-learning applications in digital multimedia analysis, wireless communication, and signal-processing applications in multimedia.

MOHAMMED A. SALEM (Member, IEEE) received the B.Sc. degree from the Department of Electrical Engineering, Faculty of Engineering, Higher Technological Institute, Egypt, in 2008, and the M.Sc. and Ph.D. degrees from the Department of Electronics and Electrical Communications Engineering, Faculty of Engineering, Al-Azhar University, Egypt, in 2014 and 2020, respectively. He is a peer reviewer in many conferences and SCI journals related to IEEE, Elsevier, and Springer publishers. His current research interests include IEEE 802.11-based wireless communications, the Internet of Things (IoT), 5G and beyond communication systems, medium access control, channel estimation, vehicular communications, and reconfigurable intelligent surface. He is a program committee member of many conferences.